

Ionic charge emission into fog from a remotely piloted aircraft

Article

Published Version

Creative Commons: Attribution 4.0 (CC-BY)

Open Access

Harrison, R. G. ORCID: <https://orcid.org/0000-0003-0693-347X>, Nicoll, K. A. ORCID: <https://orcid.org/0000-0001-5580-6325>, Marlton, G. J., Tilley, D. J. and Iravani, P. (2022) Ionic charge emission into fog from a remotely piloted aircraft. *Geophysical Research Letters*, 49 (19). e2022GL099827. ISSN 0094-8276 doi: 10.1029/2022GL099827 Available at <https://centaur.reading.ac.uk/107287/>

It is advisable to refer to the publisher's version if you intend to cite from the work. See [Guidance on citing](#).

To link to this article DOI: <http://dx.doi.org/10.1029/2022GL099827>

Publisher: American Geophysical Union

All outputs in CentAUR are protected by Intellectual Property Rights law, including copyright law. Copyright and IPR is retained by the creators or other copyright holders. Terms and conditions for use of this material are defined in the [End User Agreement](#).

www.reading.ac.uk/centaur

CentAUR

Central Archive at the University of Reading

Reading's research outputs online

Geophysical Research Letters[®]

RESEARCH LETTER

10.1029/2022GL099827

Key Points:

- First example of an instrumented uncrewed aerial vehicle used to release charge for fog modification
- Unipolar charge release into fog is followed by fog reflectivity increases
- Observations consistent with charge-induced droplet size distribution changes

Supporting Information:

Supporting Information may be found in the online version of this article.

Correspondence to:

R. G. Harrison,
r.g.harrison@reading.ac.uk

Citation:

Harrison, R. G., Nicoll, K. A., Marlton, G. J., Tilley, D. J., & Iravani, P. (2022). Ionic charge emission into fog from a remotely piloted aircraft. *Geophysical Research Letters*, 49, e2022GL099827. <https://doi.org/10.1029/2022GL099827>

Received 23 FEB 2022

Accepted 30 AUG 2022

Author Contributions:

Conceptualization: R. Giles Harrison, Keri A. Nicoll

Data curation: R. Giles Harrison, Keri A. Nicoll

Funding acquisition: R. Giles Harrison, Keri A. Nicoll

Methodology: R. Giles Harrison, Keri A. Nicoll

Project Administration: R. Giles Harrison, Keri A. Nicoll, Pejman Iravani
Resources: Graeme J. Marlton, Douglas J. Tilley, Pejman Iravani

Software: R. Giles Harrison

Supervision: R. Giles Harrison





Writing – original draft: R. Giles Harrison

Writing – review & editing: R. Giles Harrison, Keri A. Nicoll, Graeme J. Marlton, Douglas J. Tilley, Pejman Iravani

© 2022. The Authors.

This is an open access article under the terms of the [Creative Commons Attribution License](#), which permits use, distribution and reproduction in any medium, provided the original work is properly cited.

Ionic Charge Emission Into Fog From a Remotely Piloted Aircraft

R. Giles Harrison¹ , Keri A. Nicoll^{1,2} , Graeme J. Marlton^{1,3} , Douglas J. Tilley⁴ , and Pejman Iravani^{4,5}

¹Department of Meteorology, University of Reading, Berkshire, UK, ²Department of Electronic and Electrical Engineering, University of Bath, Bath, UK, ³Now at MetOffice, Exeter, UK, ⁴Department of Mechanical Engineering, University of Bath, Bath, UK, ⁵Now at Volant Autonomy, Bath, UK

Abstract Charge influences the properties of liquid droplets, such as evaporation rates, hydrodynamic stability, and sticking probabilities. Modifying droplet charge therefore provides a possible method of influencing fogs or clouds. An instrumented, remotely piloted aircraft has been equipped with positive and negative corona emitters to cause droplet charging. With the aircraft circling at 20 m altitude, effects of ion release were compared in clear air and natural fog. In clear air, the surface atmospheric electrical field changed whenever the emitters were activated, but without significant differences in the short-wave radiation as the aircraft passed over previously ionized air. In fog, radiation fluctuations showed a Gaussian distribution before either emitter operated or when both emitters were operating, but with different distributions during unipolar ion emission. Introducing unipolar ions led to a maximum change in fog reflectivity of ~2%, about 25 s later.

Plain Language Summary Methods to influence fogs and clouds are potentially useful for weather modification, hence new or neglected approaches are worth evaluating. For example, it has long been known that water droplets behave differently if they are electrically charged, and more inclined to stick to each other when they collide. These effects have rarely, if ever, been investigated with natural clouds, partly because of difficulties in accessing clouds to release the charge and in assessing any resulting changes. These problems can be overcome using uncrewed electrically powered aircraft, piloted from the ground individually or flown autonomously as a fleet. Small wingspan aircraft are well suited for this, as, unlike liquid and chemical sprays, charge release does not require significant payloads of extra material, and the aircraft propulsion batteries can provide the charge. A small aircraft carrying measurement equipment has been specially developed to investigate this. With it, charge release experiments have been undertaken in a natural fog, using a circling flight pattern to detect changes following the charge release. Positive or negative charge released separately was found to increase the fog's reflection of sunlight, indicating that charge can influence cloud properties in a variety of situations.

1. Introduction

Water droplets in air occur commonly in clouds and fogs. The droplets act to remove the molecular cluster-ions generated by radioactivity and cosmic rays. Through this attachment process, droplets acquire a net charge (Gunn, 1954). This can influence their behavior, for example, through modifying collisions and evaporation (Harrison & Ambaum, 2008; Khain et al., 2004). Introducing charge artificially may therefore provide a method of influencing natural droplet systems, with potential applications to fog dispersal, rainfall enhancement or modifying cloud reflectivity (Harrison et al., 2015). In situ investigation through direct experimentation on a natural fog is described here, using an aircraft for charge release.

Clouds and fogs are sensitive systems where droplet growth rates and size distributions are important properties. Small changes, for example, in droplet sizes can lead to cloud brightening (Hobbs et al., 2000). Electrical influences on droplet behavior have long been recognized (Strutt, 1879), with recent modeling showing that charge-enhanced collection hastens droplet growth to raindrop sizes (Ambaum et al., 2022; Guo & Xue, 2021). Charging a droplet until the electrical force generated exceeds the droplet's surface tension, will lead to physical disruption and fragmentation (Duft et al., 2003; Rayleigh, 1882). Modifying charges in clouds has been attempted by releasing corona ions upwards from the surface, for investigation of cloud electrification (Vonnegut et al., 1962) and weather modification (Wilderer et al., 2011). Charge release can now be achieved into clouds

and fogs from above and within, using uncrewed aerial vehicles (UAVs) (Harrison et al., 2021). Following experiments injecting negative charge into surface fog (Harrison et al., 2022), fog experiments are described using the UAV bipolar charge emission technology for the first time.

Droplets charge by collecting ions (Gunn, 1954). Following a transient burst of ions, a drop may obtain a large charge, which is sufficient to cause physical disruption by the electrical force overcoming the surface tension, that is, exceeding the *Rayleigh limit* (Duft et al., 2003; Rayleigh, 1882). When ion concentrations are steady rather than transient, diffusion of ions to droplets leads to a steady-state charge distribution. For droplets of a single radius r , this charge distribution—the modified Boltzmann distribution (Clement & Harrison, 1991)—gives the number concentration of droplets carrying j elementary charges N_j as a fraction of the neutral droplet concentration N_0 , by

$$\frac{N_j}{N_0} = x^j \frac{\sinh(\lambda j)}{j} \exp(-\lambda j^2) \quad (1)$$

where $\lambda = \frac{e^2}{8\pi\epsilon_0 r k_B T}$ with ϵ_0 is the permittivity of free space, k_B is Boltzmann's constant, T is the temperature, and e is the elementary charge. The important quantity x is the ion asymmetry ratio, given by $x = \left[\frac{n_+ \mu_+}{n_- \mu_-} \right]$ for positive and negative ion concentration n_+ and n_- respectively, and electrical mobility μ_+ and μ_- . As bipolar ion mobilities are typically similar, the droplet charge distribution away from transient sources principally depends on the relative number concentrations of negative and positive ions. From Equation 1, the mean number of elementary charges, j_m on a droplet is given by

$$j_m = \frac{1}{2\lambda} \ln(x) \quad (2)$$

(Gunn, 1954). Hence, by increasing n_+ or n_- through introducing ions to modify x , the mean droplet charge can be changed.

Fog presents accessible experimental circumstances in which ion concentrations can be modified by release from a small aircraft. Fog droplets are typically smaller than cloud droplets, often in the diameter range 1–10 μm (Pilié et al., 1975; Pruppacher et al., 1998) for which electrical effects are proportionally greater (Harrison et al., 2015). Such experiments are, however, challenging, both because practical deployment of an aircraft in fog is difficult, and because the operators need to travel safely to the site in potentially hazardous weather conditions before the fog dissipates. In addition, the limited visual range requires safe flying procedures to be developed and approved beforehand. An unpopulated valley where fog was known to occur was chosen for this work, near Castle Cary in the southwest UK (51.09788°N, 2.486905°W). A fixed surface monitoring system was established at the site to record droplet size distributions and the atmospheric electric field.

In Section 2, the experiments, instrumentation and methodology are described, and results presented in Section 3. Section 4 provides further discussion, with conclusions in Section 5.

2. Experiment Description

These experiments used an aircraft executing circular horizontal flight above a measurement site, where droplet properties and electric field were monitored. Positive and negative charge emitters were activated on the aircraft in a repeated sequence. Changes in visible radiation below were monitored from an on-board optical sensor in a fixed position looking downward. For analysis, the radiative responses observed were grouped by different combinations of emitters operating.

2.1. Instrumentation

The surface monitoring system consisted of an electric field mill to measure the potential gradient (PG), and a Light Optical Aerosol Counter, LOAC (Renard et al., 2016) to determine aerosol and droplet concentrations. PG values were obtained at 1 s sampling, with the LOAC providing droplet number concentrations on 1 min scans, across 19 unequal size bins from 0.2 to 50 μm .

The aircraft used was a catapult-launched Skywalker X8 carrying monitoring instruments (Harrison et al., 2021). These included meteorological sensors, an optical cloud sensor (Harrison & Nicoll, 2014), and wide dynamic range charge sensors (Harrison et al., 2017) on each wing. To release charge as unipolar and bipolar ions, the aircraft carried

Table 1
Summary of Flights and Their Circumstances

Flight no	Date	Duration (UTC)	Conditions	Incoming ^a solar radiation (W m ⁻²)	Sunrise and sunset times ^b (UTC)	Air temperature ^c at 2 m (°C)	Surface pressure ^c (hPa)
2	26 February 2021	1015 to 1030	After fog dissipation	182	0702 1744	3	1,035
4	26 February 2021	1505 to 1520	Clear air	209	0702 1744	6	1,035
5	27 February 2021	0750 to 0815	Fog	31	0700 1746	3	1,040
7	9 March 2021	0821 to 0835	Murky air	147	0636 1805	6	1,020

^aFound in flights 2, 4, and 7 when the aircraft banked away from circling and throughout flight 5 (See Supporting Information S1). ^bFound from <https://www.timeanddate.com>. ^cECMWF reanalysis for 06 UTC and 12 UTC.

corona emitters. A positive emitter under one wing and a negative emitter under the other delivered an ion current into the aircraft's wake of nominally $\pm 1 \mu\text{A}$. The corona emitters were specifically designed for this aircraft, with configurable operating voltage and corona current (Harrison et al., 2021) although no attempt was made at accurate current balancing. The emitters were activated manually from the ground using aircraft control telemetry. Data from all the sensors, together with the state of the emitters and the aircraft position, were subsequently time-aligned and combined. (Figure S1 in Supporting Information S1 provides an equipment overview).

2.2. Methodology

Days on which measurements were potentially possible were anticipated using weather forecasts, with the final decision on flight operations made early in the morning concerned, following team discussions. The UAV and sensors were then readied rapidly for flight operations.

Take-off and landing were under pilot control, with the circling flight pattern pre-programmed into the autopilot, at 20 m above the surface. The rotations were clockwise as viewed from above the aircraft, of 200 m diameter and 20 s duration, with the aircraft speed 30 ms^{-1} , and part of the flight circle passed over the surface instruments. Due to limited propulsion battery capacity, and initial manual flight required to establish safe operation, a maximum of about 30 circles could be obtained per flight. Once the circling pattern was established the emitters were activated. The switching sequence used was (a) positive emitter on with negative emitter off, (b) negative emitter on with positive emitter off, and (c) both emitters on, for 20 s on and off in each case, timed manually to help randomize the starting positions. The sequences (a), (b), and (c) were repeated for as long as possible. This approach was taken to generate multiple separate experiments in the same circumstances, to reduce the effect of natural variability. Data were later analyzed considering different combinations of the emitters on and off.

The Optical Cloud Sensor (OCS) flown on the UAV contains a downward-looking visible photodiode (type VT8440) and amplifier (Harrison & Nicoll, 2014). The photodiode views downward from the aircraft's nose, to detect reflected solar radiation. It detects from 300 to 1,100 nm, with a response time of typically $10 \mu\text{s}$ (RS-Online, 2004), and a 16-bit radiation resolution of 25 mW m^{-2} .

3. Results

Four flights were undertaken which deployed the new technology for the first time, in a range of quiescent anti-cyclonic circumstances including fog, summarized in Table 1. During the flights, the LOAC droplet counter and field mill operated at the surface. On 26 February 2021, flight 2 followed clearance of early morning fog, with flight 4 during the afternoon. On 27th February, flight 5 was made in fog but within visual sight, during continued anticyclonic conditions with negligible surface wind. On 9th March, flight 7 was made after fog had lifted. (The surface droplet size distributions obtained are shown in Figures S2, S3–S6 in Supporting Information S1 show the flights' solar radiation measurements, from which radiation fluctuations were derived for analysis.) Radiation

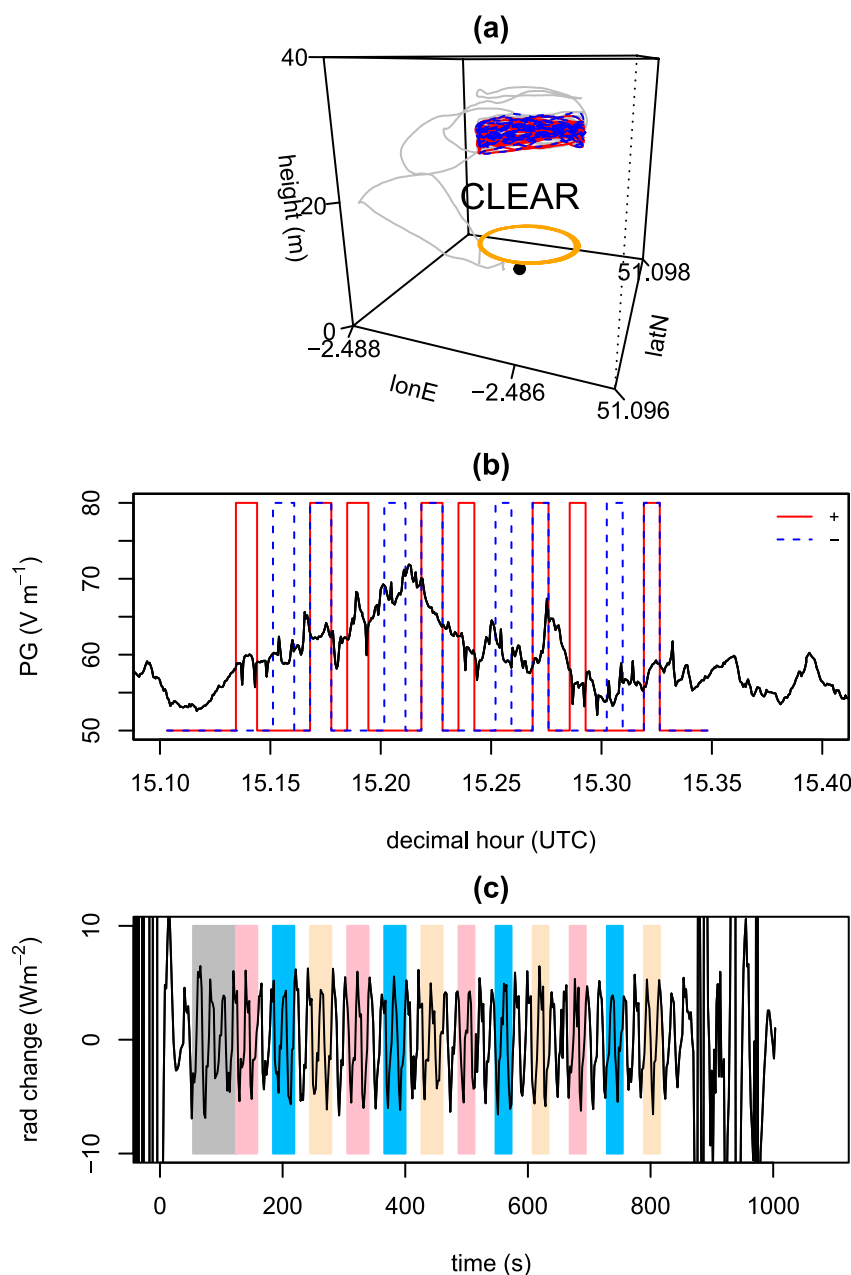


Figure 1. (a) Aircraft trajectory during clear air flight 4 (gray lines), around and above the surface field mill (the black dot), with the circular flight pattern projected onto the surface (orange lines). (b) Time series of surface Potential Gradient (PG) and (c) detrended downward-looking photodiode radiation measurements. In (a), the trajectory is marked in red or blue when the positive or negative charge emitter was operating, and in (b) switching of the positive and negative charge emitters is marked with red or dotted blue lines, respectively. In (c), the pre-emission reference period of photodiode variability is identified with gray shading, and operating times of the positive, negative, and both charge emitters with pink, blue, and beige shading, respectively.

data from other flights (2 and 7) do not show the rotation-induced fluctuations as clearly as in flight 4, suggesting that increased diffuse solar radiation occurred from droplets or particles. Flight 4 was concluded to be the most representative clear air flight, for comparison with the fog flight.

Figures 1 and 2 summarize flights 4 and 5, for clear and foggy air, respectively. In panel (a) of each figure, the aircraft GPS-derived trajectory is shown, in which the circular flight above the surface instruments is evident. The trajectories are marked in red or blue whenever the positive or negative emitters were operating, respectively.

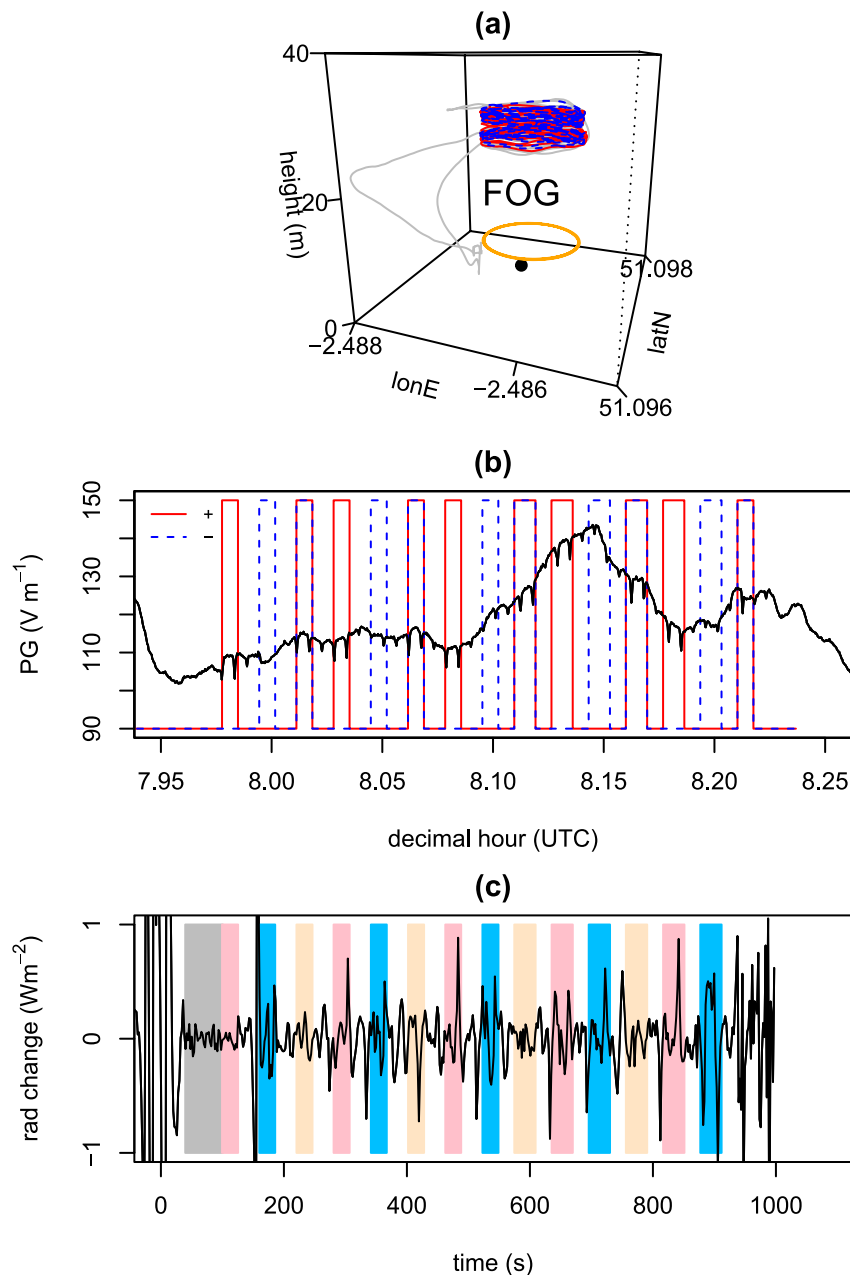


Figure 2. As for Figure 1, but for the fog flight, flight 5.

Each panel (b) provides simultaneous PG data from the surface field mill, together with the emitter switching. Small PG transients are apparent as the aircraft passes overhead. In each panel (c), fluctuations in visible radiation measured by the aircraft photodiode are shown. For the clear air case, these variations are consistent with solar radiation changes from repeated circular loiters of the UAV in sunlight; in the foggy air case, there is much reduced magnitude variation, and the detrended trace is less uniform, with changes apparent around emitter switching times. Previously, radiative measurements made within clouds using the same photodiode have shown notably little variability (Harrison & Nicoll, 2014) and good temperature stability (Nicoll & Harrison, 2012).

Figure 3 shows data from the same two flights, with a more detailed comparison of the photodiode signals. The photodiode variations are for (a and d) positive emitter only, (b and e) negative emitter only, and (c and f) both emitters activated. The radiation variations are for the second circular rotation after the relevant emitter was

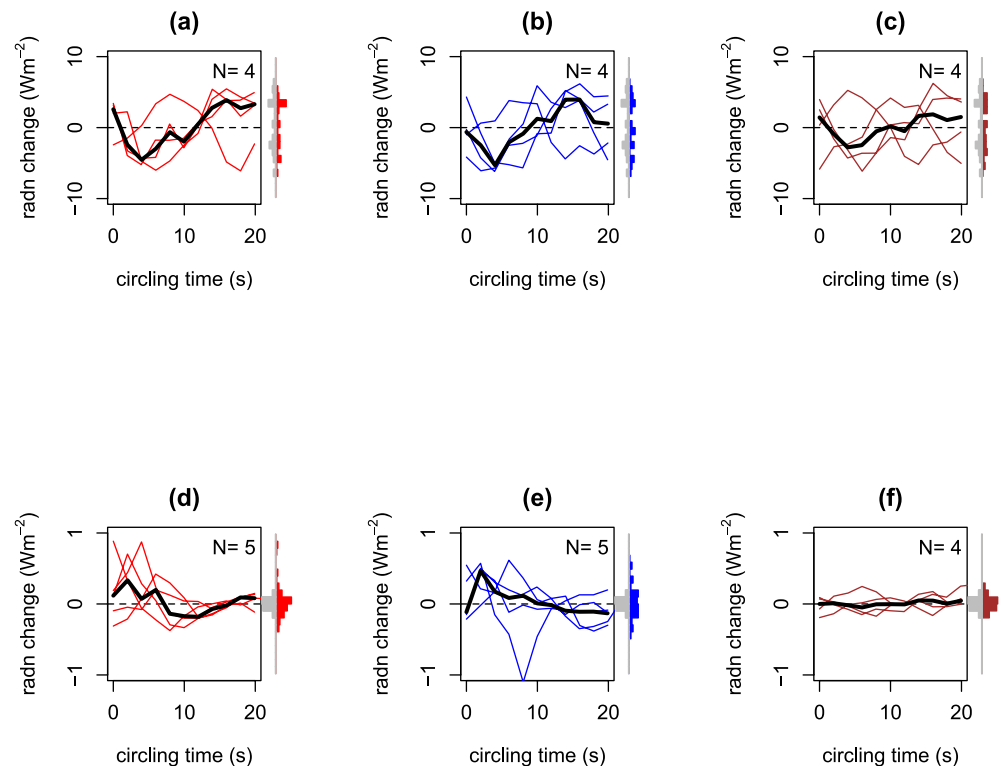


Figure 3. Radiation changes from the downward-looking aircraft photodiode during circular loiters, for clear conditions (a, b, and c) and fog (d, e, and f). Measurements were made during the second circle after (a and d), only the positive emitter was switched on, (b and e) only the negative emitter was switched on and (c and f) both emitters were switched on. Each thin line represents one rotation, with the median (thick line) derived from N repeated trials. Right-hand margin histograms show radiation values obtained across all the circular loiters, contrasted with reference values (gray bars) during aircraft circling before emitter activation.

switched on. This ensures that the photodiode samples air beneath, at the first step change where ions were introduced, with the least ion dispersion by the wind. A short period after the circular flight pattern was established, but before the emitters were activated—identified in Figures 1c and 2c as the gray boxed region—is used to provide reference radiation variations, for comparison with emitters on.

For the clear air flight, the photodiode signals are essentially indistinguishable between the cases when either emitter is operating separately (Figures 3a and 3b) or when both (Figure 3c) emitters are operating. They also have similar variations to the reference period when neither emitter was operating. Histograms of radiation fluctuations in each case do not show significant differences, using a Kolmogorov-Smirnov (KS) statistical test. This is consistent with no expectation of radiative effect of ions in clear air, in the wavelength range of the photodiode.

In the fog flight, however, differences emerge between the different situations. Figures 3d and 3e show the radiation fluctuations with the positive or negative emitter operating separately. In either case the variability is much greater than for the reference period, and there is an increase in reflected radiation in the first 5 s of the second circle, that is, up to 25 s after the emitter was activated. The enhanced reflectivity declines thereafter, suggesting it is not due to droplet attraction by aircraft charging, which would steadily increase with operating time of the emitters. Additionally, the delayed observation well after emitter activation, with a slow rise and fall of the reflectivity, indicates the photodiode response is not caused by a switching transient across the aircraft systems.

With both emitters operating (Figure 3f), the variability is much reduced compared with either emitter operating separately. The histograms of the radiation fluctuations also appear different between these cases. Statistical tests indicate that (a) the radiation fluctuations are not normally distributed for the positive emitter on

(Shapiro-Wilk, SW test, $p < 10^{-3}$), nor for the negative emitter on (SW test, $p = 0.02$), but (b) that radiation fluctuations with both emitters on and during the reference periods are normally distributed. Further, (c) the normally distributed radiation fluctuations with both emitters on and the reference period have different variability (F -test, $p < 0.04$). Finally, (d) the radiation fluctuations in the negative emitter case are different from the reference period fluctuations (KS test, $p < 0.05$). These measurements were made within an hour of sunrise (Table 1), but sunrise artifacts, such as a spectral change, are unable to explain the variations, due to the multiple emitter operations. Sunlight-related effects are considered further in Figure S7 in Supporting Information S1. In the clear air case, the radiation fluctuations vary strongly with rotation angle, but a similarly strong rotation effect does not occur during fog. This supports the radiation effects in fog originating from emitter operation.

4. Discussion

The statistical tests (1–4) demonstrated that using the emitters separately leads to a different distribution of radiation fluctuations, compared with either the case of both emitters operating, or with no ion emission. Radiation fluctuations in the latter two cases are normally distributed, indicative of random variations, but they are nevertheless different, suggesting that the bipolar ions have a small effect compared with no ion emission.

The radiation fluctuations are combined and summarized in Figure 4a. These are found from the distribution width (inter-quartile range), normalized by the width of the reference period radiation fluctuations for the flight concerned. These ratios show that the fog flight is markedly different from the other three flights, and that using the emitters separately in fog has a different effect on the reflected radiation from using them together. For both the fog and “murky” flights, there is a greater range of radiation fluctuations for the negative emitter than for positive, and the least range when both emitters were used. As the emitters were operated on a regular but interleaved pattern, the repeated emitter operations in the fog flights amount to undertaking multiple experiments in the same circumstances.

Overall, an increase in fog reflectivity was observed beneath the aircraft after the introduction of unipolar ions, with a median change initially of about 0.5 Wm^{-2} . Considering the background solar radiation during the flight (31 Wm^{-2}), the maximum change in reflectivity is $\sim 2\%$. The reflectivity is proportional to the total droplet area, hence such a change could result from a shift in the droplet size distribution to larger droplets, or an increase in their number, or both.

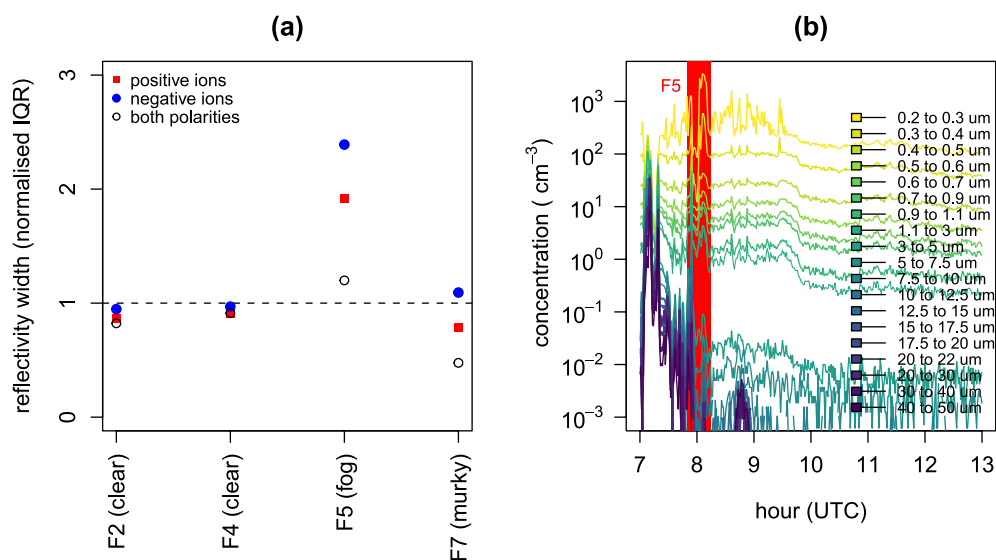


Figure 4. (a) Width (inter-quartile range, IQR) of photodiode radiation fluctuation histograms compared for the four flights F2, F4, F5, and F7, with different emitter configurations, normalized by the IQR of the photodiode variability during each flight's reference period. (b) Surface droplet concentrations in fog, with flight 5 identified by the red background. Each colored line on (b) refers to a concentration time series from an individual LOAC size bin, given by the legend.

Further information is available from the LOAC surface measurements (see also Figure S2 in Supporting Information S1). Figure 4b shows LOAC droplet data around flight 5 (fog), during which the larger ($>10\text{ }\mu\text{m}$ diameter) droplet concentrations decreased, but the smaller ($<5\text{ }\mu\text{m}$ diameter) droplets increased and became more variable. This suggests an increase in smaller droplets accompanied the observed reflectivity effects, also not inconsistent with small droplet generation observed after unipolar ion emission into surface fogs (Harrison et al., 2022).

The difference in the radiation responses between unipolar ionization of either polarity compared with bipolar ionization is important. From Equation 2, the mean charge of droplets is given by the ratio of the positive to negative ion concentration. If only positive or negative ions are emitted the asymmetry factor will change (i.e., $x \gg 1$ or $x \ll 1$, respectively), leading to a droplet charge distribution with a substantially non-zero mean charge. For approximately comparable emission rates of both ion polarities, $x \approx 1$ and the mean charge will be small, but the timescale to steady-state charge distribution will be more rapid. Reduced droplet charging with bipolar emission would be expected to have less effect on the fog, as observed. Hence, the fog reflectivity enhancement can be associated with introduction of unipolar ions, on timescales of a few tens of seconds. This is consistent with a process linked to droplet charging from ion concentration asymmetry, either transiently close to the aircraft, or in the steady-state, some distance from the emitters.

Bounding estimates of the steady-state droplet charge are possible. The beamwidth of the VT8440 photodiode (to one-half response) is $\pm 50^\circ$ (RS-Online, n.d.), defining a swath of $\pm 23\text{ m}$ at the surface below the aircraft flying at 20 m . At 30 ms^{-1} flight speed, the associated volume swept out per unit time is $1.5 \times 10^4\text{ m}^3\text{ s}^{-1}$. For an emission current of $1\text{ }\mu\text{A}$ (6.3×10^{12} ions s^{-1}) into the same volume, about 400 ions cm^{-3} would be generated, or about 4 elementary charges e per droplet for the LOAC-observed surface concentration of $100\text{ droplets cm}^{-3}$. These estimates are for mean values well away from the ion sources: close to the emitters, the drop charging would be very much greater, and in laboratory experiments with a levitated drop, smaller emitter currents have been shown to charge drops to their Rayleigh limit (Airey et al., 2021). Near to the emitter without significant dispersion, $1\text{ }\mu\text{A}$ can charge 1 m^3 of $1\text{ }\mu\text{m}$ diameter droplets at a concentration of $100\text{ droplets cm}^{-3}$, to their Rayleigh limit ($45,000\text{ }e$) each second. This would cause immediate disintegration and generation of smaller droplets.

5. Conclusions

Release of unipolar ions into a fog from an UAV has been observed to be associated with transient changes in the fog's radiative properties and reflectivity. Such properties depend primarily on the droplet size distribution. The radiative changes can therefore be explained through charge-induced modifications to the droplet size distribution. In contrast to unipolar ions, introducing bipolar ions will lead to a relatively small mean droplet charge, but hastening the time to a steady-state charge distribution.

These results are the first to demonstrate charge release into fog from robotic aircraft, potentially providing a new route to influence clouds and fogs without generation of chemical residues. Charged droplets also occur naturally, hence droplet charge fluctuations associated with variability in the global atmospheric electric circuit and space weather may also lead to cloud and fog droplet size distribution changes.

Data Availability Statement

The data files generated are available at <https://doi.org/10.17864/1947.000358>.

Acknowledgments

This material is based on the work supported by the National Center of Meteorology, Abu Dhabi, UAE under the UAE Research Program for Rain Enhancement Science (UAEREP). KAN acknowledges a NERC Independent Research Fellowship (NE/L011514/1) and (NE/L011514/2). Stefan Chindea, Freddie Sherrat, David Cleaver, and Jonathan du Bois helped with the flights and associated permissions. We thank the landowner of Bottom Barn Farm. Analysis was undertaken using R (R core team, 2021).

References

- Airey, M. W., Harrison, R. G., Aplin, K. L., & Pfrang, C. (2021). Effects of ionisation on cloud behaviour in planetary atmospheres. In *Geophysical Research Abstracts*. <https://doi.org/10.5194/egusphere-egu21-13639>
- Ambaum, M. H. P., Auerswald, T., Eaves, R., & Harrison, R. G. (2022). Enhanced attraction between drops carrying fluctuating charge distributions. *Proceedings of the Royal Society A: Mathematical, Physical & Engineering Sciences*, 478(2257). <https://doi.org/10.1098/rspa.2021.0714>
- Clement, C. F., & Harrison, R. G. (1991). Charge distributions on aerosols. *Institute of Physics Conference Series*, 118, 275–280.
- Duft, D., Achtzehn, T., Müller, R., Huber, B. A., & Leisner, T. (2003). Coulomb fission: Rayleigh jets from levitated microdroplets. *Nature*, 421(6919), 128. <https://doi.org/10.1038/421128a>
- Gunn, R. (1954). Diffusion charging of atmospheric droplets by ions, and the resulting combination coefficients. *Journal of Meteorology*, 11(5), 339–347. [https://doi.org/10.1175/1520-0469\(1954\)011<0339:dcoadb>2.0.co;2](https://doi.org/10.1175/1520-0469(1954)011<0339:dcoadb>2.0.co;2)
- Guo, S., & Xue, H. (2021). The enhancement of droplet collision by electric charges and atmospheric electric fields. *Atmospheric Chemistry and Physics*, 21(1), 69–85. <https://doi.org/10.5194/acp-21-69-2021>

- Harrison, R. G., & Ambaum, M. H. P. (2008). Enhancement of cloud formation by droplet charging. *Proceedings of the Royal Society A: Mathematical, Physical & Engineering Sciences*, 464(2098), 2561–2573. <https://doi.org/10.1098/rspa.2008.0009>
- Harrison, R. G., Marlton, G. J., Ambaum, M. H. P., & Nicoll, K. A. (2022). Modifying natural droplet systems by charge injection. *Physical Review Research*, 4(2), L022050. <https://doi.org/10.1103/physrevresearch.4.022050>
- Harrison, R. G., Marlton, G. J., Nicoll, K. A., Airey, M. W., & Williams, P. D. (2017). Note: A self-calibrating wide range electrometer for in-cloud measurements. *Review of Scientific Instruments*, 88(12), 126109. <https://doi.org/10.1063/1.5011177>
- Harrison, R. G., & Nicoll, K. A. (2014). Note: Active optical detection of cloud from a balloon platform. *Review of Scientific Instruments*, 85(6), 066104. <https://doi.org/10.1063/1.4882318>
- Harrison, R. G., Nicoll, K. A., & Ambaum, M. H. P. (2015). On the microphysical effects of observed cloud edge charging. *Quarterly Journal of the Royal Meteorological Society*, 141(692), 2690–2699. <https://doi.org/10.1002/qj.2554>
- Harrison, R. G., Nicoll, K. A., Tilley, D. J., Marlton, G. J., Chindea, S., Dingley, G. P., et al. (2021). Demonstration of a remotely piloted atmospheric measurement and charge release platform for geoengineering. *Journal of Atmospheric and Oceanic Technology*, 38(1), 63–75. <https://doi.org/10.1175/JTECH-D-20-0092.1>
- Hobbs, P. V., Garrett, T. J., Ferek, R. J., Strader, S. R., Hegg, D. A., Frick, G. M., et al. (2000). Emissions from ships with respect to their effects on clouds. *Journal of the Atmospheric Sciences*, 57(16), 2570–2590. <https://doi.org/10.1175/1520-0469>
- Khain, A., Arkhipov, V., Pinsky, M., Feldman, Y., & Ryabov, Y. (2004). Rain enhancement and fog elimination by seeding with charged droplets. Part I: Theory and numerical simulations. *Journal of Applied Meteorology*, 43(10), 1513–1529. <https://doi.org/10.1175/JAM2131.1>
- Nicoll, K. A., & Harrison, R. G. (2012). Balloon-borne disposable radiometer for cloud detection. *Review of Scientific Instruments*, 83(2), 025111. <https://doi.org/10.1063/1.3685252>
- Pilié, R. J., Mack, E. J., Kocmond, W. C., Eadie, W. J., & Rogers, C. W. (1975). The life cycle of valley fog. Part II: Fog microphysics. *Journal of Applied Meteorology*, 14(3), 364–374. [https://doi.org/10.1175/1520-0450\(1975\)014<0364:tlcovf>2.0.co;2](https://doi.org/10.1175/1520-0450(1975)014<0364:tlcovf>2.0.co;2)
- Pruppacher, H. R., Klett, J. D., & Wang, P. K. (1998). Microphysics of clouds and precipitation. *Aerosol Science and Technology*, 28(4), 381–382. <https://doi.org/10.1080/02786829808965531>
- Rayleigh, L. (1882). On the equilibrium of liquid conducting masses charged with electricity. *The London, Edinburgh, and Dublin Philosophical Magazine and Journal of Science*, 14(87), 184–186. <https://doi.org/10.1080/14786448208628425>
- R Core Team. (2021). R: A language and environment for statistical computing. R Foundation for Statistical Computing, Vienna, Austria. Retrieved from <https://www.R-project.org/>
- Renard, J. B., Dulac, F., Berthet, G., Lurton, T., Vignelles, D., Jégou, F., et al. (2016). LOAC: A small aerosol optical counter/sizer for ground-based and balloon measurements of the size distribution and nature of atmospheric particles-Part 1: Principle of measurements and instrument evaluation. *Atmospheric Measurement Techniques*, 9(4), 1721–1742. <https://doi.org/10.5194/amt-9-1721-2016>
- RS-Online. (2004). VTB process photodiode datasheet. Retrieved from <https://docs.rs-online.com/ead3/0900766b80052d0e.pdf>
- Strutt, J. W. (1879). The influence of electricity on colliding water drops. *Proceedings of the Royal Society of London*, 28, 405–409. <https://doi.org/10.1098/rspl.1878.0146>
- Vonnegut, B., Moore, C. B., Stout, G. E., Staggs, D. W., Bullock, J. W., & Bradley, W. E. (1962). Artificial modification of atmospheric space charge. *Journal of Geophysical Research*, 67(3), 1073–1083. <https://doi.org/10.1029/JZ067i003p01073>
- Wilderer, P. A., Davydova, E., & Saveliev, Y. (2011). Abstraction of atmospheric humidity. *Treatise on Water Science*, 4, 111–145. <https://doi.org/10.1016/B978-0-444-53199-5.00079-8>